https://doi.org/10.5194/egusphere-2025-4213
Preprint. Discussion started: 9 October 2025

Is earlier always better? A comparative assessment of rainfall replenishment timing for multiyear drought mitigation

Yichen Zhang[1], Fubao Sun[2], Wenbin Liu[2], Jie Zhang[1*], Wenli Lai[3], Jiquan Lin[4], Wenchao Sun[5], Wenjie Liu[1], Zhongyi Sun[1], Peng Wang[1]

[1]School of Ecology, Hainan University, Haikou, 570228, China
[2]Key Laboratory of Water Cycle and Related Land Surface Processes, Institute of Geographic Sciences and Natural Resources Research, Chinese Academy of Sciences, Beijing, 100101, China
[3]School of Geography and Environmental Sciences, Hainan Normal University, Haikou, 571158, China
[4]Hainan Provincial Ecological Environment Monitoring Center, Haikou 571126, China
[5]College of Water Sciences, Beijing Normal University, Xinjiekouwai Street 19, Beijing, 100875, China

Corresponding to: Jie Zhang (zhang_jie@hainanu.edu.cn)

Abstract. Multiyear droughts (MYDs) are recognized as severe drought events, with especially profound impacts on both human activities and ecosystems. However, the optimal rainfall replenishment timing ($t_{optimal}$) for MYDs mitigation remains insufficiently understood. With that in mind, we conducted a retrospective analysis of historical MYDs based on the Palmer Drought Severity Index (PDSI) in China during 1961-2020, and the calibration period was set to 1961-1990. We performed a series of numerical experiments involving precipitation gradient increases for 351 selected MYDs, distributed across 199 grids (2° × 2°), from 1991 to 2020, and developed a drought mitigation quantitative model (DMQM). In addition, a key coefficient (*k*) derived from DMQM was defined to quantify the mitigation efficiency, and toptimal was then identified as the timing corresponding to the maximum *k* (k_{max}). Overall, drought severity exhibits a nonlinear response to increased precipitation. k_{max} occurred most frequently in the first month of drought onset (t_1), accounting for 58.79% of all grids, while the second (t_2) and third (t_3) months were also non-negligible, accounting for 22.11% and 11.06%, respectively. Compared to the humid river basins in southern China, the arid and semi-arid northern regions had a higher probability for *k* at t_2 or t_3 to exceed *k* at t_1. Drought duration (DD) was identified as a key factor, as longer DD was associated with a greater likelihood of t_2 or t_3 being the toptimal, evidenced by R^2 values of 0.526 and 0.578, respectively. These findings contribute to ensuring timely and regionally appropriate MYD mitigation strategies and interventions.

1 Introduction

Droughts are recognized as a major natural hazard with profound negative effects on both human activities and the environment (Berdugo et al., 2020; Shi et al., 2021; Palagi et al., 2022). Compared to other natural hazards, droughts often rank higher in key characteristics of losses, such as total loss of life and total economic loss (Mishra and Singh, 2010). For instance, in the United States, drought caused $250 billion in damages and nearly 3,000 deaths between 1980 and 2020, making them the costliest and second deadliest natural disaster (Ault, 2020). In Europe, drought-related financial losses over

https://doi.org/10.5194/egusphere-2025-4213
Preprint. Discussion started: 9 October 2025

the three decades prior to 2007 were estimated to exceed EUR 100 billion (Blauhut et al., 2016). In China, prolonged droughts in Southwest China during 2018-2020 resulted in economic losses of $240 million, underscoring the intensifying impacts of prolonged droughts (Feng et al., 2025). Such devastating drought events, which typically last more than 12 months (Brunner and Tallaksen, 2019; Mourik et al., 2025), are referred to as multiyear droughts (MYDs). Under climate change, these persistent, expansive, and difficult-to-recover MYD events have shown an escalating trend in severity, duration, and frequency (Dai, 2013; Zhang et al., 2016; Stevenson et al., 2022; Chen et al., 2025; Wang et al., 2025).

Droughts are primarily related to prolonged reductions in the precipitation for a region (McCabe and Wolock, 2015; Hao et al., 2018; Zhang et al., 2021). For instance, the Millennium Drought in southeast Australia (2001-2009) was the longest drought on record for the region (Van Dijk et al., 2013). Similarly, the California droughts from 2012 to 2015 included the driest three-year period on record in the state (2012-2014) (Mao et al., 2015; Luo et al., 2017). The MYD in Europe from 2014 to 2018 was also record-breaking for the region (Moravec et al., 2021; Büntgen et al., 2021). To better quantify the severity of drought, various drought indices have been developed based on deviations in water availability against long-term normal conditions. Currently, the most widely used drought indices include the Palmer Drought Severity Index (PDSI), Standardized Precipitation Evapotranspiration Index (SPEI), and Standardized Precipitation Index (SPI) (Zhang et al., 2016; Liu et al., 2017; Mukherjee et al., 2021). These indices typically quantify drought severity on a monthly timescale based on precipitation and/or potential evapotranspiration (PET) (Easterling et al., 2007; Vicente-Serrano et al., 2010). They generally standardize monthly effective precipitation time series under the assumption of a normal distribution, enabling the identification of thresholds that delineate different drought intensities (Dai, 2011; Vicente-Serrano et al., 2025). Moreover, by thoughtfully incorporating auto-correlation processes (such as auto-correlation coefficients or the accumulation of antecedent water deficit/surplus), these indices can effectively capture the dynamic evolution of typical drought events, including their onset, development, recovery, and termination (Gupta and Karthikeyan, 2024). To further characterize the dynamic evolution of typical drought events, Yevjevich (1967) proposed the run theory, which extracts drought features from three key dimensions. These include: (a) Drought duration (DD, the period during which a drought parameter is continuously below the critical threshold), (b) Drought intensity (DI, the lowest index value during a drought event), (c) Drought severity (DS, the cumulative deficiency of a drought parameter below the critical threshold throughout the event). Such drought indicators have been widely applied at station, regional, and global scales to assess drought processes and related impacts (Gu et al., 2020; Wu et al., 2022; Ullah et al., 2022; Zhou et al., 2023), with DS particularly offering a more integrated measure of drought impact (Cavus and Aksoy, 2020).

Previous studies have examined the dynamic evolution of drought events across the four stages (Ma et al., 2023; Lin et al., 2023). It has been widely observed that the recovery and termination phases are often accompanied by increased precipitation (Haile et al., 2020). However, such hydrometeorological changes typically occur several months after the onset of severe drought, by which time substantial ecological, agricultural, and socioeconomic damages may have already occurred (DeChant and Moradkhani, 2015; Livneh and Hoerling, 2016; Wu et al., 2018). For example, in southeast Australia, the Millennium Drought (2001-2009) was terminated by unusually high rainfall in early 2010, yet this MYD still exhibited

https://doi.org/10.5194/egusphere-2025-4213
Preprint. Discussion started: 9 October 2025

prolonged DD and high DS (Yang et al., 2017). Consequently, earlier precipitation replenishment is more effective in mitigating drought impacts (Fig. 1a and 1b). From another perspective, drought indices typically represent anomalies from normal conditions in a standardized way, allowing comparisons across space and time. This implies that during extreme drought, when the index deviates far from zero, even small increases in precipitation can trigger substantial shifts toward recovery. In contrast, during mild drought, when the index remains near zero, the same amount of precipitation leads to only marginal improvement. For instance, using the widely applied PDSI as an example, to induce the same one-unit change in the index, the required shift in cumulative probability under extreme drought (PDSI = -4) is only 48% of that under milder conditions (PDSI = -1) (Fig. 1c and 1d). This illustrates the nonlinear sensitivity of drought indices to precipitation inputs: index responses to identical precipitation replenishment can vary significantly depending on drought severity. However, such nonlinear responses are often overlooked. Small increases in precipitation during extreme drought are frequently dismissed as inconsequential, despite their potential to drive meaningful recovery (Pan et al., 2013). Zhang et al. (2024) noted that the effect of a 1% precipitation increase on drought recovery probability under extremely dry conditions is 13.2 times greater than under extremely wet conditions.

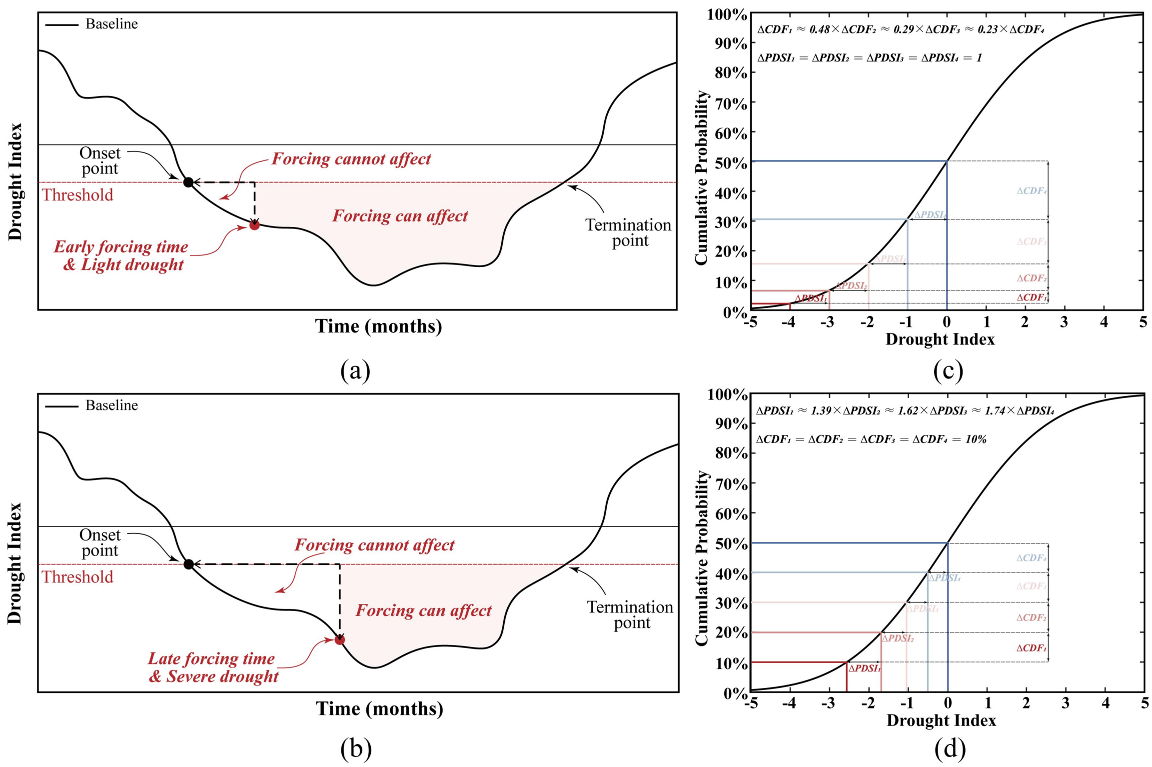

Figure 1: Conceptual and statistical illustrations related to drought mitigation and the normal distribution characteristics of commonly used drought indices (with PDSI as an example). (a) Drought severity is relatively mild during the early stages of a drought event. (b) Severe droughts are generally associated with longer duration. (c) Change in cumulative probability induced by a one-unit shift in PDSI under varying drought intensity. (d) PDSI shift required to achieve an equivalent change in cumulative probability under different drought conditions.

https://doi.org/10.5194/egusphere-2025-4213
Preprint. Discussion started: 9 October 2025

Currently, the optimal timing ($t_{optimal}$) for drought mitigation remains insufficiently understood. Several existing studies focus on early drought monitoring, as well as on mitigation measures implemented during severe drought (Haile et al., 2020). However, we suggest that effective drought mitigation may not necessarily occur at either of these two stages. In particular, cases where early precipitation replenishment and drought severity are considered together remain under-investigated. Therefore, it is necessary to clarify the relationship between different rainfall replenishment timings ($t_{forcing}$) and drought mitigation. To this end, we propose a new framework (Fig. 3) involving a series of numerical experiments to retrospectively investigate typical historical MYD events. Section 2 introduces the study area and datasets. In Section 3, representative MYD events are identified based on existing literature, with a particular focus on assessing the extent of drought mitigation during these events. A model based on increased precipitation forcing applied at different stages of MYD is developed to parameterize mitigation efficiency. The accuracy of this parameter is validated by comparing model-derived estimates with the results of independent numerical experiments. The results and related discussion are presented in section 4 and section 5. We close with a brief conclusion in Section 6.

2 Study area and datasets

To assess the role of nonlinear patterns in MYD mitigation, we utilize a daily meteorological dataset suitable for calculating PDSI during the period of 1961 to 2020 over China. This dataset includes precipitation (pr), air temperature (mean, maximum, and minimum), relative humidity, wind speed, and sunshine duration. This dataset consisting of 756 stations is provided by the National Climate Centre of the China Meteorological Administration and has been quality-controlled before being released to the scientific community (http://www.nmic.gov.cn/). Given the importance of reliable statistics, we applied additional temporal and spatial consistency control on the data based on the information of the length of available data (and the missing data) and the density of stations, etc. First, we have done temporal consistency control using the information of data length and select 620, out of the 756, meteorological stations with continuing measurements. The 620 stations are distributed in 10 large river basins covering China, as shown in Fig. 2. Second, we conduct further control on the spatial inhomogeneity of station distribution. We select 199 grid boxes of $2° \times 2°$ longitude by latitude (Fig. 2), and each grid box should contain at least one station with continuing meteorological measurements. For the given grid box with multiple stations, the station results were averaged to represent the grid box. In doing that, we reduce the possible influence from temporal and spatial inhomogeneities in the data and ensure that the overall statistics are robust.

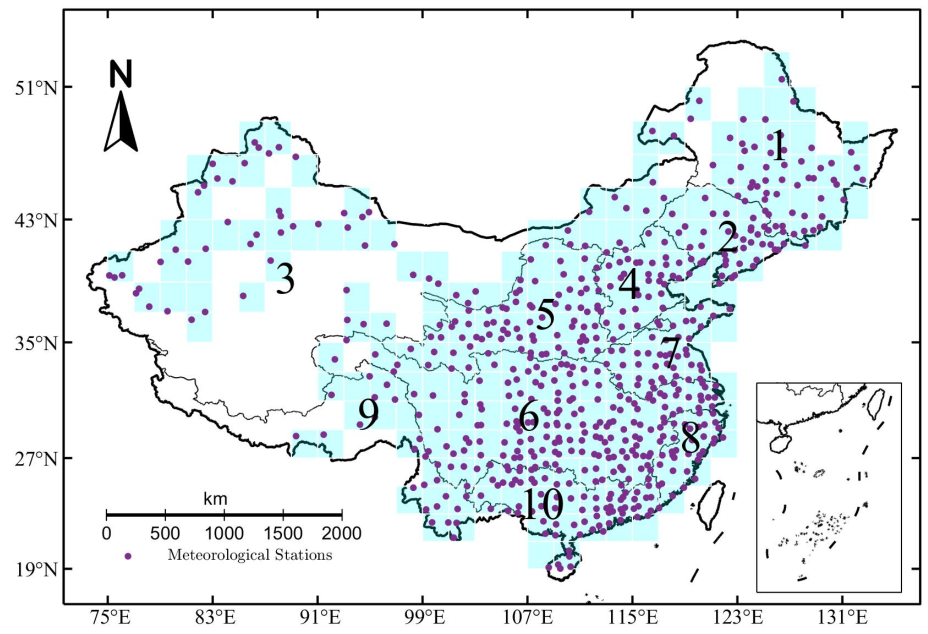

Figure 2: The study area covers 10 large river basins (regions). No. 1, the Songhua River; No. 2, the Liao River; No. 3, Northwestern Rivers; No. 4, the Hai River; No. 5, the Yellow River; No. 6, the Yangtze River; No. 7, the Huai River; No. 8, Southeastern Rivers; No. 9, Southwestern Rivers and No. 10, Pearl River. A total of 199 (2° × 2°) grid boxes (color: cyan) were identified as containing at least one station with continuous instrumental meteorological records. In total, 620 meteorological stations (purple dots) were used.

3 Methods

3.1 Overview

To determine $t_{optimal}$ for drought mitigation by jointly considering early precipitation replenishment (Conceptual Model 1 as mentioned in Section 3.4) and drought severity (Conceptual Model 2 as mentioned in Section 3.4), we propose the following methodological framework (Fig. 3). We calculate the PDSI using data from meteorological stations, identify representative MYD events and characterize them in terms of DS, DD, DI, Drought Development Period (DDP), and Peak Intensity Point (PIP). The framework consists of the following three steps: (1) Validation of the nonlinear response of DS to increased precipitation forcing applied incrementally along a gradient; (2) Construction of a novel drought mitigation quantitative model (DMQM); (3) Verification of the applicability of the key parameter derived from the DMQM: k, the mitigation efficiency coefficient. The $t_{optimal}$ is then determined based on the timing at which k reaches its maximum value (k_{max}). Finally, we evaluate the impact of $t_{forcing}$ on drought mitigation. A detailed description of each methodological component is provided in the subsequent sections.

https://doi.org/10.5194/egusphere-2025-4213
Preprint. Discussion started: 9 October 2025

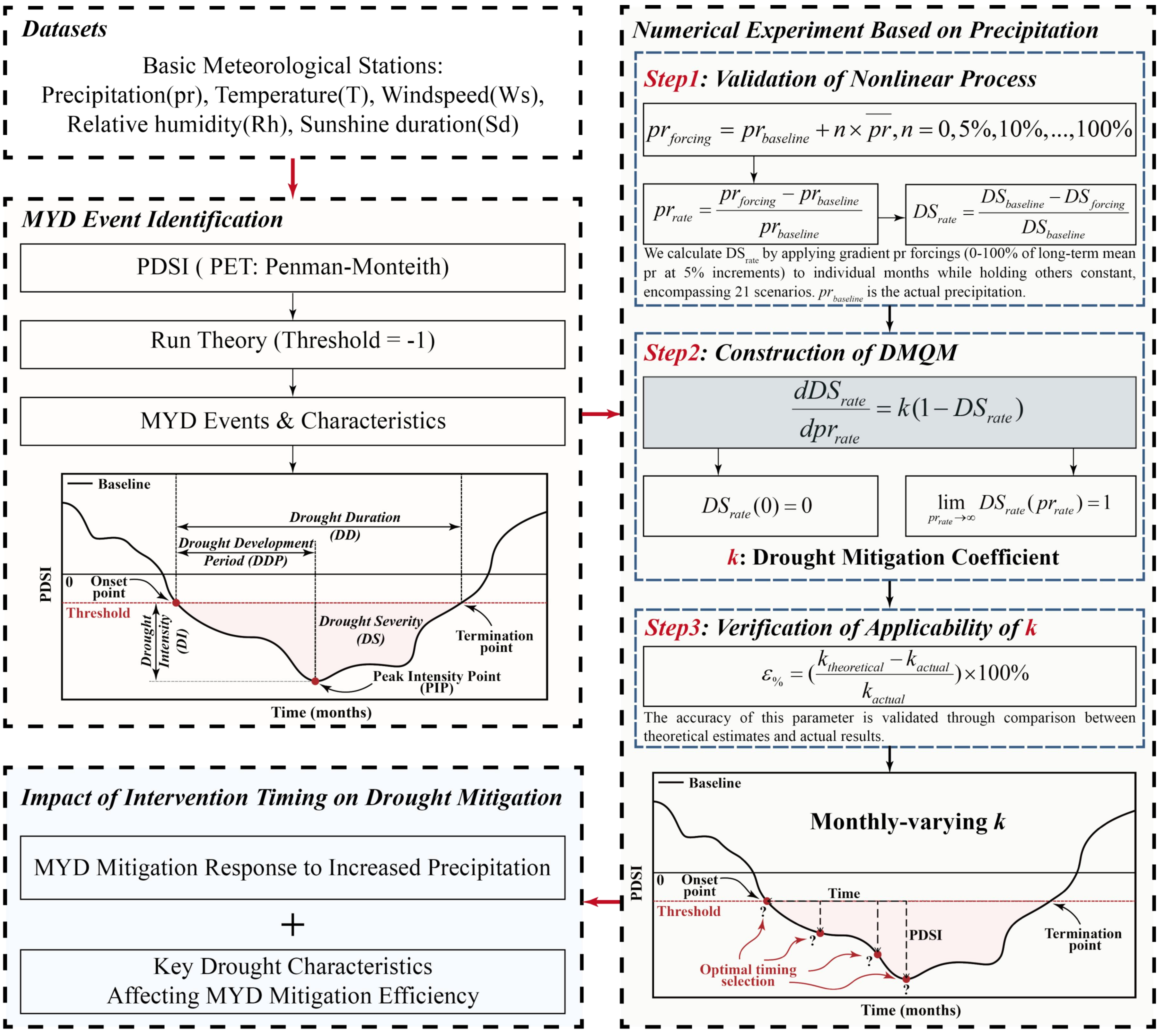

Figure 3: Workflow and method overview.

3.2 Estimation of PDSI using the Penman-Monteith method

In this study, PDSI was used to quantify the deviation between observed monthly precipitation and the required precipitation, which is estimated each month under Climatically Appropriate For Existing Conditions (CAFEC). It was improved using a simple two-layer water balance model (Palmer, 1965), which considered water supply and atmospheric evaporative demand. To ensure the credibility of PDSI results, we use the Penman-FAO56 method with a physical mechanism (Xu et al., 2022) to estimate the potential evapotranspiration (denoted as *PET_pm*):

https://doi.org/10.5194/egusphere-2025-4213
Preprint. Discussion started: 9 October 2025

$$PET\_pm = \frac{0.408 \cdot \Delta \cdot (R_n - G) + \gamma \cdot \frac{900}{T + 273} \cdot U_2 \cdot e_s \cdot (1 - Rh/100)}{\Delta + \gamma \cdot (1 + 0.34 \cdot U_2)} \tag{1}$$

Where Δ is the slope of the vapor pressure curve, R_n is the net radiation (calculated using surface downwelling/upwelling shortwave/longwave radiation), G is the soil heat flux, γ is the psychometric constant, T is the monthly averaged air temperature, U_2 is the wind speed at 2m height, e_s is the saturation vapor pressure at a given air temperature, Rh is the relative humidity.

In this study, long-term PDSI series for the period 1961-2020 were calculated using the tool provided by the Palmer Drought Severity Index (Jacobi et al., 2013). The calibration period was set to 1961-1990 to calculate the CAFEC values, thereby ensuring that PDSI thresholds remain fixed throughout the analysis.

3.3 Identification and characterization of MYD events based on run theory

Run theory is a threshold-based method that defines drought events as the values of PDSI less than -1 (Yang et al., 2024), and extracts such events from the monthly PDSI time series of each grid. According to this method, each identified drought event was further characterized by a set of indicators, including DS, DD, DI, DDP, and PIP (Fig. 4a). In this study, based on the characteristics of typical MYD events (Chen et al., 2025), the identified events were further selected according to the criteria of $\mathrm{DD} > 12$ and $\mathrm{DI} < -3$. Since the calibration period was set to 1961-1990 and the CAFEC values needed to remain fixed during numerical experiments, the final selection was restricted to MYD events occurring between 1991 and 2020. A total of 351 MYD events meeting these criteria were identified. Each basin contained at least 11 events, thereby helps ensuring the statistical robustness of the analysis.

3.4 Design of numerical experiments to quantify the precipitation-based mitigation efficiency of MYD

According to run theory, for a given drought event characterized by its baseline monthly PDSI series (Fig. 4a), an increase in precipitation applied at a specific month will inevitably lead to a reduction in DS, assuming all other conditions remain unchanged. This provides a foundation for evaluating mitigation efficiency based on changes in DS. The $t_{forcing}$ is a key parameter representing the timing of the applied forcing. In the numerical experiment, $t_{forcing}$ is denoted as t_m, where t_m refers to the m-th month of MYD. For instance, t_1 represents the first month of MYD. Two conceptual models are proposed to characterize different patterns of mitigation efficiency. Conceptual Model 1 features the same precipitation forcing applied at different $t_{forcing}$ during an MYD event (Fig. 4b). Since the forcing can only influence DS from the $t_{forcing}$ and thereafter, earlier rainfall replenishment allows a longer duration to affect the drought process. Thus, $t_{optimal}$ under Conceptual Model 1 (denoted as t_a) approaches the beginning of the event, i.e., $t_a \rightarrow t_1$. Conceptual Model 2 features the same precipitation forcing applied at the same $t_{forcing}$, but under different PDSI values (Fig. 4c). As a standardized index, the PDSI associates greater negative values (i.e., more severe drought conditions) with more substantial DS reductions following rainfall

https://doi.org/10.5194/egusphere-2025-4213
Preprint. Discussion started: 9 October 2025

replenishment, indicating higher mitigation efficiency. Therefore, $t_{optimal}$ under Conceptual Model 2 (denoted as t_b) tends to coincide with the timing of PIP (denoted as t_{PIP}), i.e., $t_b \rightarrow t_{PIP}$. To determine a composite $t_{optimal}$ (denoted as t_c), which integrates patterns described in both Conceptual Model 1 and Conceptual Model 2, we designed a series of numerical experiments involving precipitation gradient increases at different $t_{forcing}$ (Fig. 4d). Since t_c remains undetermined, it is essential to first define a plausible time range in which it may occur. Given that the t_{PIP} of MYD events typically occurs much later than the onset ($t_{PIP} \gg 1$), the t_c is expected to range from t_1 to t_{PIP}.

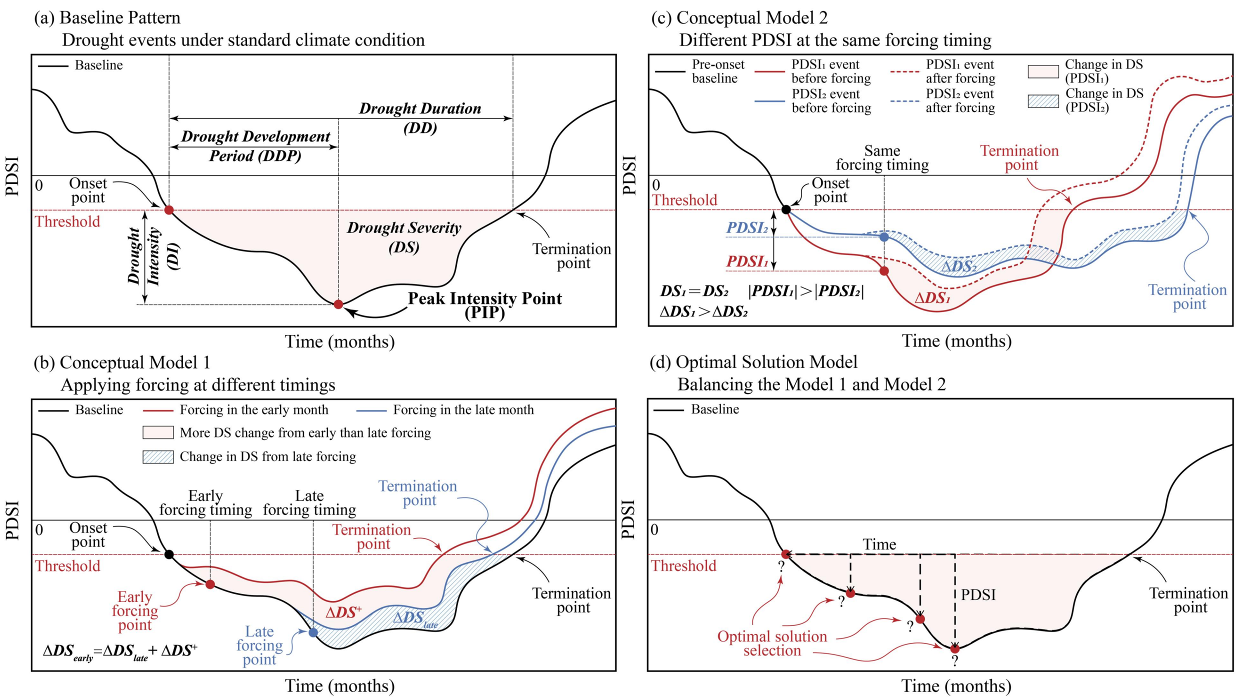

Figure 4: Conceptual models illustrating MYD mitigation driven by increased precipitation forcing: (a) Baseline pattern without increased forcing. *DS* is represented by the area of the red region. (b) Conceptual model 1: Same forcing applied at different $t_{forcing}$ during an MYD event. Early rainfall replenishment leads to greater mitigation benefits (ΔDS^{+}, red area) and avoids additional losses from cumulative precipitation deficits. (c) Conceptual model 2: The same forcing applied at the same $t_{forcing}$, but with different drought index values. Since drought indices typically represent anomalies from normal conditions in a standardized way, deeper droughts tend to exhibit greater mitigation effects ($\Delta DS_1 > \Delta DS_2$). (d) Optimal solution model: By weighing the mismatch influences of precipitation forcing in Conceptual models 1 and 2, $t_{optimal}$ (marked by the red point) can be identified.

Since this study focuses on drought mitigation, only precipitation increase scenarios with incremental gradients are considered. The procedures of this numerical experiment were given as follows:

Step 1: Validation of nonlinear process

To validate the nonlinear response of MYD mitigation to increased precipitation forcing applied at different $t_{forcing}$ and under varying PDSI values, a single-timing precipitation forcing approach was employed. In this forcing scenario, precipitation is increased at only one $t_{forcing}$ within the event, while all other periods remain unchanged. Since the baseline scenario in this

https://doi.org/10.5194/egusphere-2025-4213
Preprint. Discussion started: 9 October 2025

185 study corresponds to the period 1961-1990 and all numerical experiments were conducted for events occurring after 1990, there is no temporal overlap between the two periods. Consequently, the baseline remains fixed throughout all gradient-based numerical experiments. The forcing approach for a given event (1991-2020) is expressed as follows:

$$pr_{forcing} = pr_{baseline} + n \times \overline{pr},\ n = 0, 5\%, 10\%, \ldots, 100\% \qquad (2)$$

Where $pr_{forcing}$ is the precipitation in the targeted month after applying the forcing, $pr_{baseline}$ is the actual precipitation in the same month under the baseline (unforced) scenario, $\overline{pr}$ is the long-term mean monthly precipitation, and $n \times \overline{pr}$ is the
190 applied precipitation forcing.

As described above, applying precipitation forcing alters the DS of the corresponding MYD event. Therefore, the relationship between $pr_{forcing}$ and the resulting change in DS can be used to validate the existence of a nonlinear response process.

Step 2: Construction of DMQM

195 To further parameterize the mitigation efficiency at individual $t_{forcing}$ of MYD, the following model was developed:

$$\frac{\partial DS_{rate}}{\partial pr_{rate}} = k \cdot (1 - DS_{rate}) \qquad (3)$$

Where DS_{rate} ($= \frac{DS_{baseline} - DS_{forcing}}{DS_{baseline}}$, $DS_{baseline}$ is the actual *DS* under the baseline scenario, and $DS_{forcing}$ is the *DS* after the precipitation forcing is applied) is the relative change in *DS*. pr_{rate} ($= \frac{pr_{forcing} - pr_{baseline}}{pr_{baseline}}$) is the relative change in precipitation.

k is the mitigation efficiency coefficient, defined as the proportionality constant between the unit residual *DS* (unmitigated
200 DS) and the drought mitigation rate.

It is clear that when no precipitation forcing is applied (pr_{rate}=0), there is no change in *DS* ($DS_{rate} = 0$). Likewise, when sufficient forcing is applied, the MYD is fully mitigated ($DS_{rate} = 1$). Thus, the model is subject to the following boundary and limiting conditions:

$$\begin{cases} DS_{rate}(0) = 0 & (4) \\ \lim_{pr_{rate} \to \infty} DS_{rate}(pr_{rate}) = 1 & (5) \end{cases}$$

Thus, based on the differential equation 3 above and the boundary and limiting conditions in equations 4 and 5, the analytical solution describing the relationship between DS_{rate} and pr_{rate} can be obtained as follows:

$$DS_{rate} = 1 - exp(-k \cdot pr_{rate}) \qquad (6)$$

Step 3: Verification of parameter applicability

To verify the applicability of the parameter, its accuracy is assessed by comparing model-derived estimates with actual values, as follows:

$$\varepsilon = \left(\frac{k_{theoretical} - k_{actual}}{k_{actual}}\right) \times 100\% \qquad (7)$$

Where ε is the relative error, $k_{theoretical}$ is the theoretical value, and k_{actual} is the actual value.

4 Results

4.1 Response relationship between DS and increased precipitation in China

The changes in DS are not proportional along the increasing precipitation gradient. Therefore, we developed the DMQM to quantitatively capture this nonlinear response (as described in Section 3.4). Focusing on drought mitigation, the numerical experiments were constrained to the $t_{forcing}$ range of DDP, with the minimum DDP among the selected MYD events being 8 months. Accordingly, t_1, t_2, ..., and t_8, represent the first to the eighth month of MYD. The corresponding k values are denoted as k_1, k_2, ..., and k_8, respectively. Within the same pr_{rate} range from 0 to 1, all timings from t_1 to t_8 exhibited a similar nonlinear response pattern. However, the maximum DS_{rate} (at $pr_{rate} = 1$) indicated that the most effective mitigation occurred during t_1 to t_3 (Fig. 5). The values of maximum DS_{rate} in the response curves for t_1 to t_3 were 0.60, 0.59, and 0.57, respectively. Correspondingly, the values of k for t_1 to t_3 were 0.92, 0.88, and 0.84, respectively, with all R^2 values exceeding 0.90. This result reflects the influence of Conceptual Model 1 as discussed in Section 3.4 (Fig. 4b), in which earlier rainfall replenishment has a greater capacity to reduce DS. In addition, we selected a gradient increase in pr_{rate} from 0 to 1 at $t_{forcing}$ as a case to observe the corresponding changes in DS_{rate}. Since PDSI values are negative during drought events, their absolute values were used to facilitate clearer comparisons. As shown in Fig. 5, the drought mitigation process can be divided into five stages based on a gradual increase in pr_{rate} from 0 to 1 (i.e., 0-0.2, 0.2-0.4, 0.4-0.6, 0.6-0.8, and 0.8-1.0). In the first stage, when pr_{rate} increases from 0 to 0.2, the absolute PDSI value at $pr_{rate} = 0.2$ is lower than that at $pr_{rate} = 0$, indicating drought mitigation. In the second stage, as pr_{rate} increases from 0.2 to 0.4, the lower absolute PDSI value reached at the end of the first stage (i.e., a milder drought) serves as the new starting point for this stage. Consequently, the initial absolute PDSI value in the second stage is lower than that in the first stage, and the same pattern applies to subsequent stages. According to

https://doi.org/10.5194/egusphere-2025-4213
Preprint. Discussion started: 9 October 2025

Conceptual Model 2 described in Section 3.4 (Fig. 4c), even when the increment in pr_{rate} is the same across two stages, a lower absolute PDSI at the beginning of the stage (i.e., a milder drought) leads to a smaller increase in DS_{rate} (Fig. 5). This explains the nonlinear response pattern observed between DS_{rate} and pr_{rate} ($\frac{d(DS_{rate})}{d(pr_{rate})} > 0, \frac{d^2(DS_{rate})}{d(pr_{rate})^2} < 0$) shown in Fig. 5. For instance, the efficiency decline at t_1 is illustrated by the blue shaded area in Fig. 5.

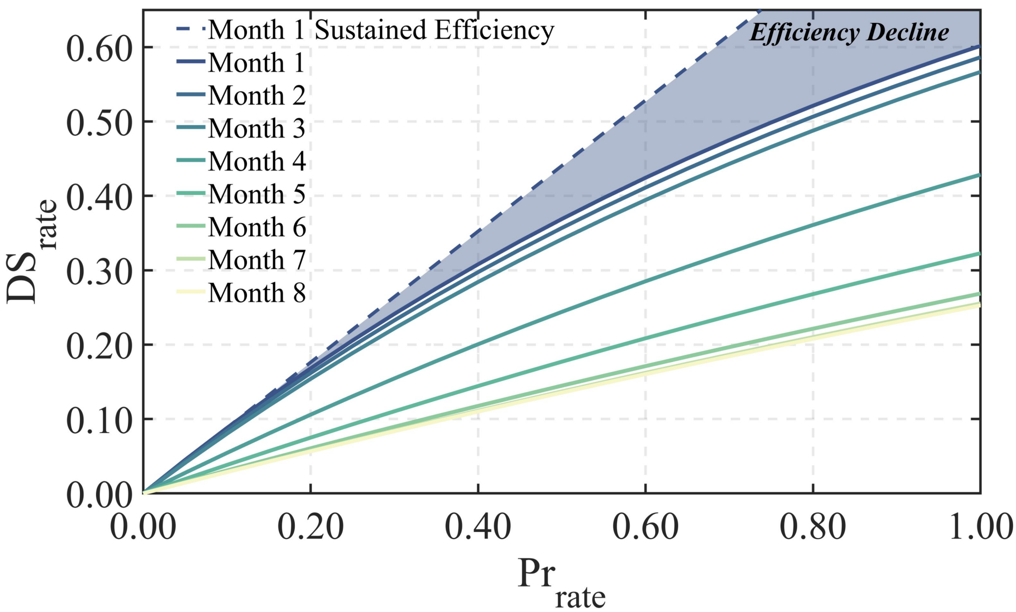

Figure 5: Nonlinear response of DS to precipitation during DDP in China. The blue area indicates the decline in mitigation efficiency in t_1 due to the nonlinear response of DS to precipitation, relative to the idealized linear response (i.e., the sustained efficiency scenario).

4.2 Validation of the mitigation efficiency coefficient in China

According to the DMQM constructed in Section 3.4, as the increment in pr_{rate} approaches zero, the corresponding DS_{rate} also approaches zero. Under this condition, the estimated value of k approaches the actual k. In other words, the actual k can be approximated using a small value of pr_{rate} (such as pr_{rate} = 0.05) and its corresponding DS_{rate}. Therefore, we calculated the actual values of k based on the DS_{rate} at pr_{rate} = 0.05. These actual values were then compared with the theoretical k values derived from the DMQM developed in Section 3.4, at the grid scale. The comparison helped to validate the applicability of the theoretical model under varying spatial conditions. Fig. 6a shows the spatial distribution of ε across all given grids, with 72.86% exhibiting a ε below 5%. This high consistency suggests that the theoretical model provides reliable estimates of drought mitigation efficiency across diverse regions. For each grid, the k_{max} (corresponding to the value of k at t_c) value was first identified. Fig. 6b then illustrates the spatial pattern of the corresponding $t_{forcing}$ at which the k_{max} occurs across the study area. Generally, t_1 dominates, accounting for 58.79% of the grids. Nonetheless, t_2 and t_3 are also non-negligible, representing

https://doi.org/10.5194/egusphere-2025-4213
Preprint. Discussion started: 9 October 2025

22.11% and 11.06%, respectively. Accordingly, we further investigate these timing-related spatial variations at the basin scale. Overall, a strong positive correlation was observed between the theoretical and actual values, with R^2 values exceeding 0.90 for t_1, t_2, and t_3 across the ten river basins in China (Fig. 6c-e). The comparison results for each month revealed no significant deviation from the 1:1 reference line, with slopes of 1.063, 1.060, and 1.037 for t_1, t_2, and t_3, respectively (Fig. 6c-e). These results demonstrate the robustness and applicability of the theoretical values at both the grid and river basin scales. For this reason, the DMQM was further employed to investigate drought mitigation efficiency at different $t_{forcing}$. Particular attention was given to how this efficiency varies when insights from Conceptual Model 1 and Conceptual Model 2 are jointly considered. This quantitative model was also used to identify $t_{optimal}$ for rainfall replenishment across t_1, t_2, and t_3.

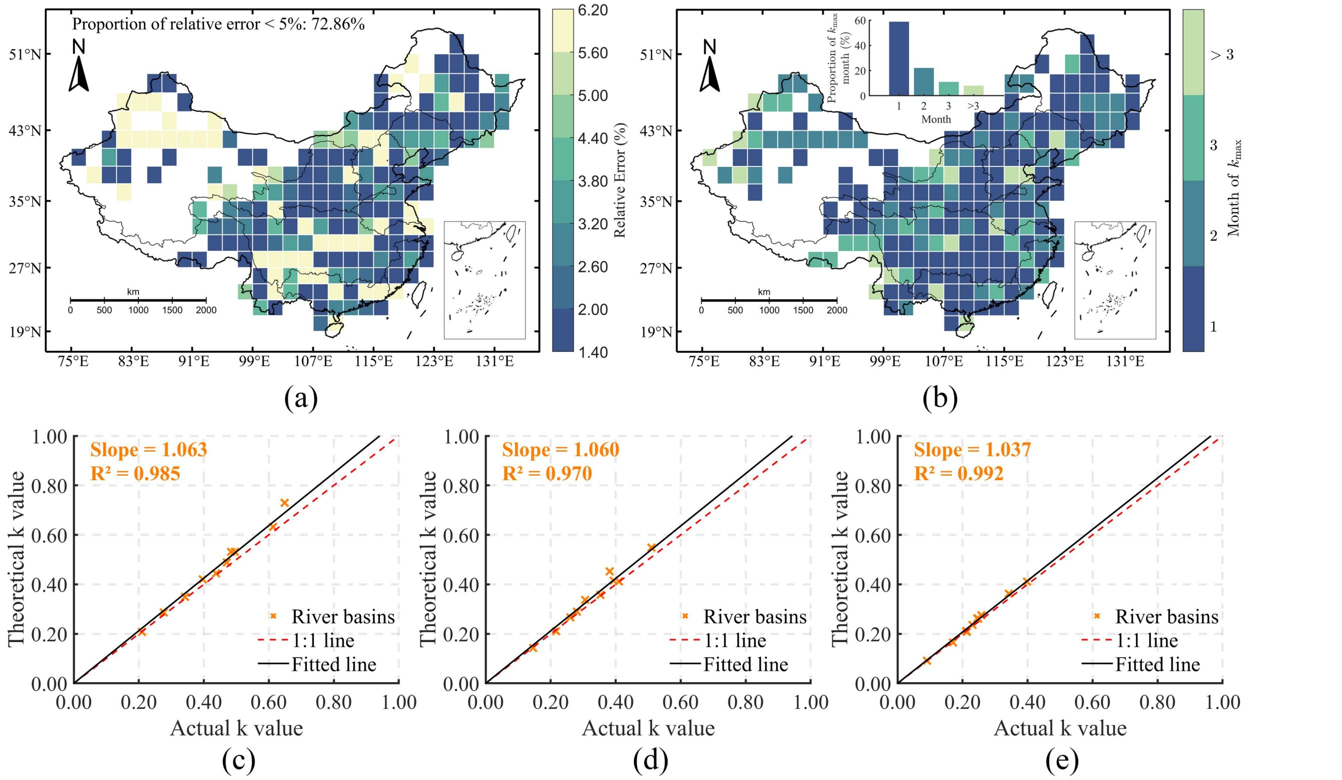

Figure 6: Verification of the applicability of k. (a) Spatial distribution of ε for each grid. (b) Spatial distribution of the timing at which the k_{max} occurs in each grid. The inset shows the frequency histogram of the timings of k_{max} values across all grids. (c-e) Median actual versus median theoretical k values for the ten major river basins in (c) t_1, (d) t_2, and (e) t_3. The red dashed line is the 1:1 line. The black solid line is the fitted line based on values from 10 river basins. Orange crosses are the values for individual river basins.

4.3 Quantification of the relationship between mitigation efficiency and rainfall replenishment timing in China

To identify $t_{optimal}$ in various river basins during t_1, t_2, and t_3, a series of numerical experiments were conducted using the DMQM. Fig. 7 presents the spatial distributions of the changes in k between t_2 and t_1 ($\Delta k_{21} = k_2 - k_1$), and between t_3 and t_1

https://doi.org/10.5194/egusphere-2025-4213
Preprint. Discussion started: 9 October 2025

($\Delta k_{31} = k_3 - k_1$). To enable a clearer comparison between negative values, their absolute values were used. Notably, the larger absolute values of negative Δk ($\Delta k < 0$) were mainly observed in the humid river basins of southern China, particularly in the Pearl River and Yangtze River basins (Fig. 7 and Table 1). By comparison, smaller absolute values of negative Δk were detected in the arid and semi-arid northern regions of China, particularly in the Liao River basin (Fig. 7 and Table 1). Moreover, in 118 out of 199 grids (59.30%), the absolute values of negative Δk_{31} were larger than those of Δk_{21} (Fig. 7 and Table 1). This disparity indicates that, in most occurrences of MYD, implementing drought mitigation measures (such as increasing effective precipitation) during the early stage of MYD events is more effective in reducing drought risks, as described in Conceptual Model 1 in Section 3.4 (Fig. 4b). Meanwhile, as shown in Fig. 7, we found that 74 out of 199 grids (37.19%) exhibited at least one positive value in either Δk_{21} or Δk_{31}. These results indicate that, in a non-negligible portion of grids, implementing drought mitigation measures at t_1 is not the optimal choice, as described in Conceptual Model 2 in Section 3.4 (Fig. 4c).

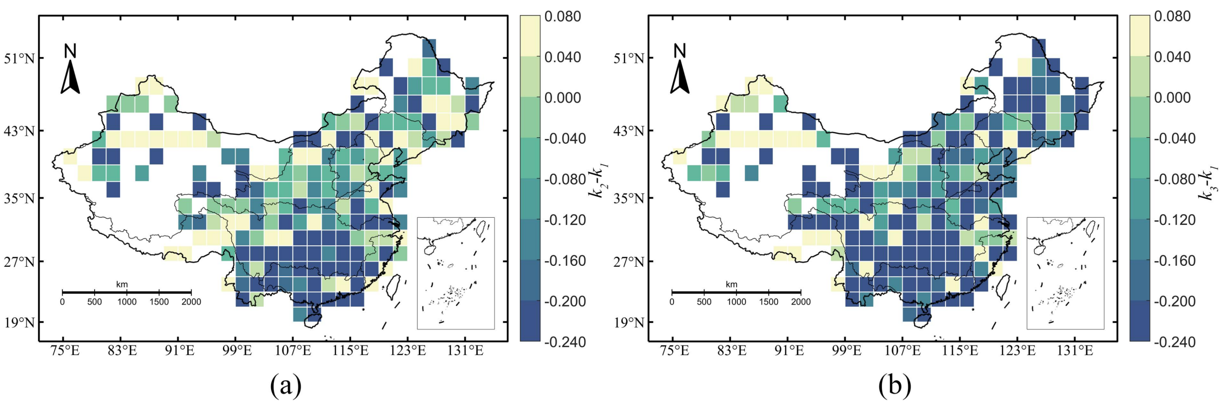

Figure 7: Spatial distribution of the changes in k (Δk). (a) Change in k between t_2 and t_1 (Δk_{21}). (b) Change in k between t_3 and t_1 (Δk_{31}).

These experiments also aimed to identify the key drought characteristics responsible for the variation in $t_{forcing}$. To this end, we summarize the probability density function (PDF) of Δk_{21}, and Δk_{31} for all of MYD events (Fig. 8 and Table 1). The Δk values exhibit a roughly normal distribution across river basins (Fig. 8). The median values of both Δk_{21} and Δk_{31} are negative in 9 out of 10 basins, with the median of Δk_{31} being lower than that of Δk_{21} (Table 1). In most basins, the standard deviation of Δk_{31} is also larger than that of Δk_{21}, indicating greater variability in the efficiency difference between t_3 and t_1 (Fig. 8). These results suggest that the efficiency advantage of early rainfall replenishment ($t_1 > t_2$ and $t_1 > t_3$). As emphasized by Conceptual Model 1, earlier drought mitigation yields greater effectiveness. This advantage becomes more pronounced when comparing t_1 and t_3. However, positive Δk_{21} and Δk_{31} values were found in 33.67% and 23.12% of all grids, respectively (Fig. 7a and 7b). Similar results were also evident in the PDFs for all of China and each individual basin (Fig. 8). These results suggest the non-negligible role of Conceptual Model 2. Longer DD tends to be associated with Δk

https://doi.org/10.5194/egusphere-2025-4213
Preprint. Discussion started: 9 October 2025

values closer to or even above zero (Fig. 8 and Table 1). In particular, the Liao River, with a second longest DD of 28 months ($DD_{all\ China} = 21\ months$), shows median Δk values of 0.022 for Δk_{21} and 0.003 for Δk_{31} (Fig. 8 and Table 1). In contrast, the Pearl River, characterized by a shorter DD of 19 months, exhibits more negative median Δk values of -0.162 and -0.200 for Δk_{21} and Δk_{31} (Fig. 8 and Table 1), respectively.

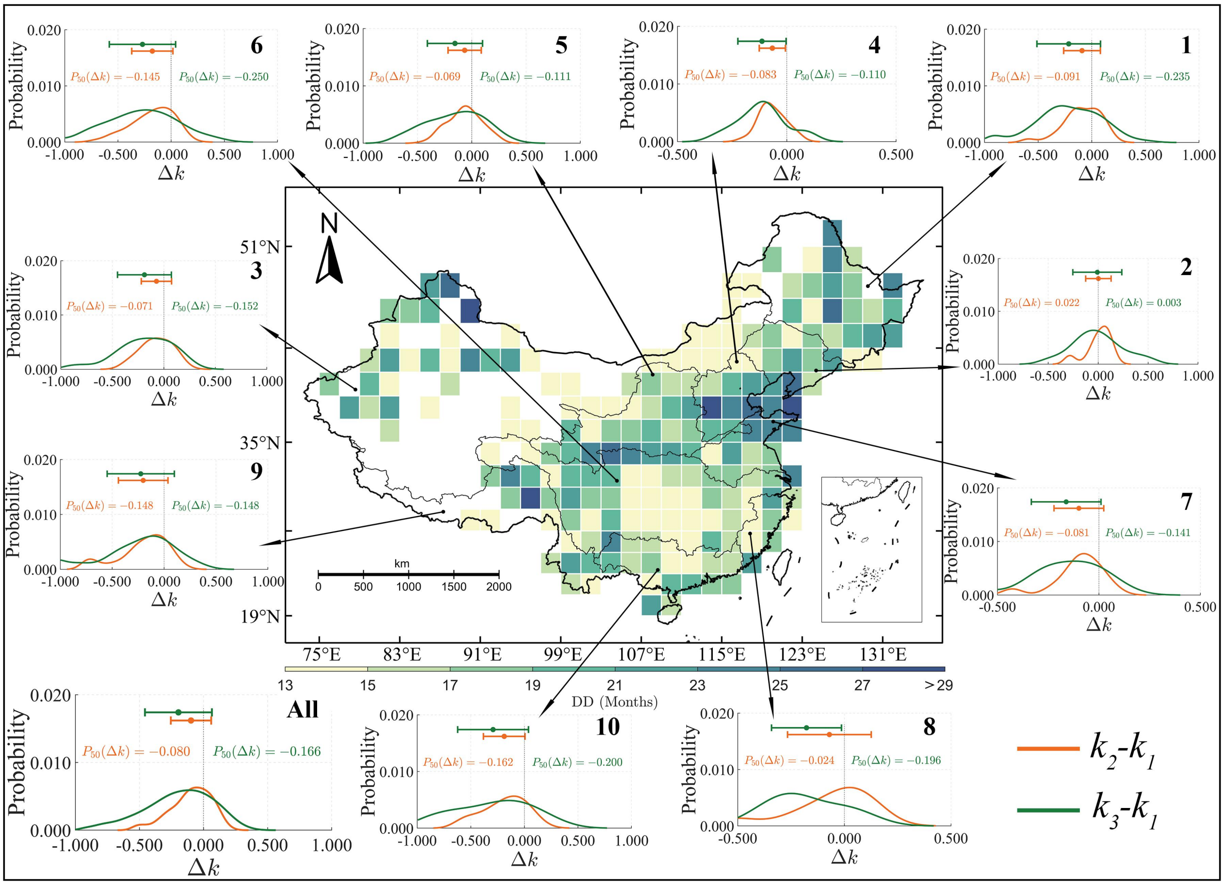

Figure 8: Spatial distribution of drought duration from 1990 to 2020 across the 10 river basins in China. Surrounding panels show the probability distribution of Δk for all of China and each basin. Specifically, the orange lines represent Δk_{21}, and the green lines represent Δk_{31}. The *x-axis* in each panel denotes Δk, while the *y-axis* denotes probability. The number in the upper-right corner of each panel indicates the basin code.

https://doi.org/10.5194/egusphere-2025-4213
Preprint. Discussion started: 9 October 2025

Table 1: Summary of the median values of DD and Δk, including Δk_{21}, Δk_{31}, and $\Delta k_{32}(= k_3 - k_2)$, across the ten river basins and all of China.

River basin	DD (Months)	$P_{50}(\Delta k_{21})$	$P_{50}(\Delta k_{31})$	$P_{50}(\Delta k_{32})$
Songhua River	22	-0.091	-0.235	-0.142
Liao River	28	0.022	0.003	-0.024
Northwestern Rivers	17	-0.071	-0.152	-0.087
Hai River	29	-0.083	-0.110	-0.053
Yellow River	21	-0.069	-0.111	-0.090
Yangtze River	19	-0.145	-0.250	-0.127
Huai River	23	-0.081	-0.141	-0.042
Southeastern Rivers	14	-0.024	-0.196	-0.077
Southwestern Rivers	21	-0.148	-0.148	-0.083
Pearl River	19	-0.162	-0.200	-0.063
All of China	21	-0.080	-0.166	-0.094

Note: red and blue numbers indicate the maximum and minimum value of P_{50} for ten river basins in China, respectively.

To further investigate the influence of DD, an equal-width binning method was applied to examine the variation of Δk under different DD values. Specifically, the original DD values of the selected MYD events ranged from 13 to 51 months. These events were grouped into bins according to their DD values. To ensure the robustness of the results (each bin contained no fewer than 10 events), the DD range was limited to 13 to 40 months, and the bin width was set to 4 months. This setting yielded a total of seven bins (Fig. 9). We calculated the median values of both Δk and DD within each bin. As shown in Fig. 9, we found a positive correlation between DD and Δk, with R^2 values of 0.526 and 0.578 for Δk_{21} and Δk_{31}, respectively. Notably, when DD exceeds 29 months (as shown in Fig. 9), the Δk values approaching zero, indicating that the mitigation efficiencies of t_2 and t_3 become comparable to that of t_1. In contrast, when DD is shorter (around 17 months, as shown in Fig. 9), t_1 demonstrates notably higher mitigation efficiency than t_2 and t_3. These results suggest that DD is a key indicator for determining $t_{optimal}$ for drought mitigation.

https://doi.org/10.5194/egusphere-2025-4213
Preprint. Discussion started: 9 October 2025

315
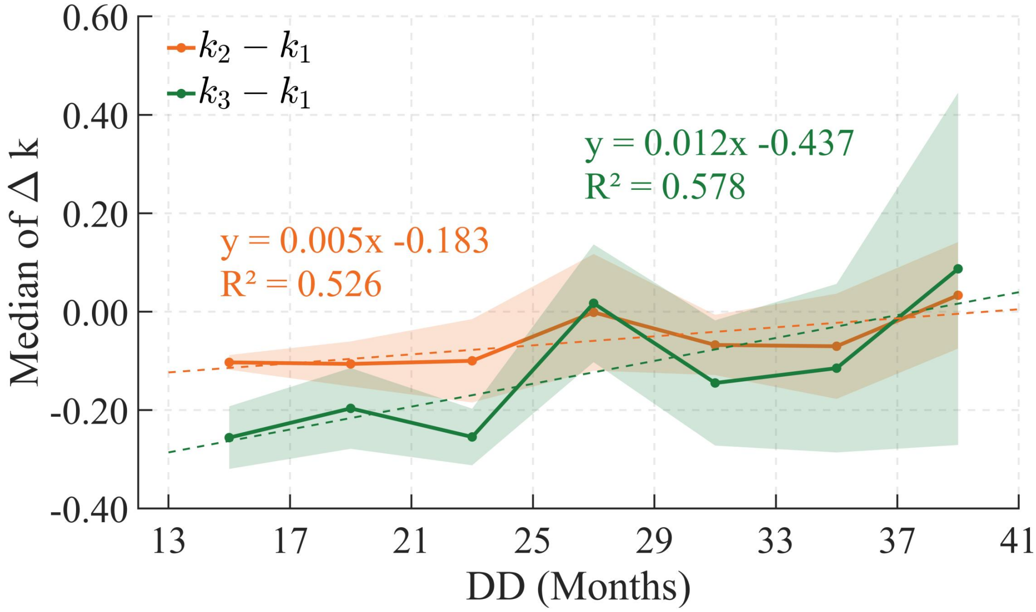

Figure 9: Median Δk of MYD under different DD. The orange line represents Δk_{21}, and the green line represents Δk_{31}. Shaded areas indicate half the standard error as the confidence interval.

To clarify the mitigation advantages of the composite $t_{optimal}$ (t_c, defined in Section 3.4), both Conceptual Model 1 and Conceptual Model 2 (as discussed in Section 3.4) were considered. Fig. 10 and Table 2 present a comparison between the
320 mitigation efficiency of t_c and those of t_a and t_b (defined in Section 3.4). The corresponding k at t_a (k_1), t_b (k_{PIP}), and t_c (k_{max}) exhibit differences. For simplicity, we define two ratios, k_{max}/k_1 and k_{max}/k_{PIP}, to quantify the differences in k between t_c and t_a, and between t_c and t_b, respectively. In terms of magnitude, k_{max}/k_1 is typically close to 1, while k_{max}/k_{PIP} consistently exceeds 2 (Table 2). From the perspective of Conceptual Model 1, t_1 tends to dominate (Fig. 10a and Table 2). Nevertheless, the presence of grids with $k_{max}/k_1 > 1$ suggests $t_{optimal} > 1$ should not be overlooked (Fig. 10a). At the basin
325 scale, t_1 dominates in most regions, except in the Liao River basin, where the median k_{max}/k_1 reaches 1.135 (Table 2). In contrast, the comparison with Conceptual Model 2 suggests that t_c offers a more substantial advantage in mitigation efficiency compared to t_{PIP} (Fig. 10b and Table 2). This advantage is particularly pronounced in the Liao River and Songhua River basins, where the median k_{max}/k_{PIP} values reach 15.430 and 12.555, respectively. By contrast, the advantage of t_c is less evident in the Southeastern River and Hai River basins, with median k_{max}/k_{PIP} values of 3.428 and 2.413, respectively.

https://doi.org/10.5194/egusphere-2025-4213
Preprint. Discussion started: 9 October 2025

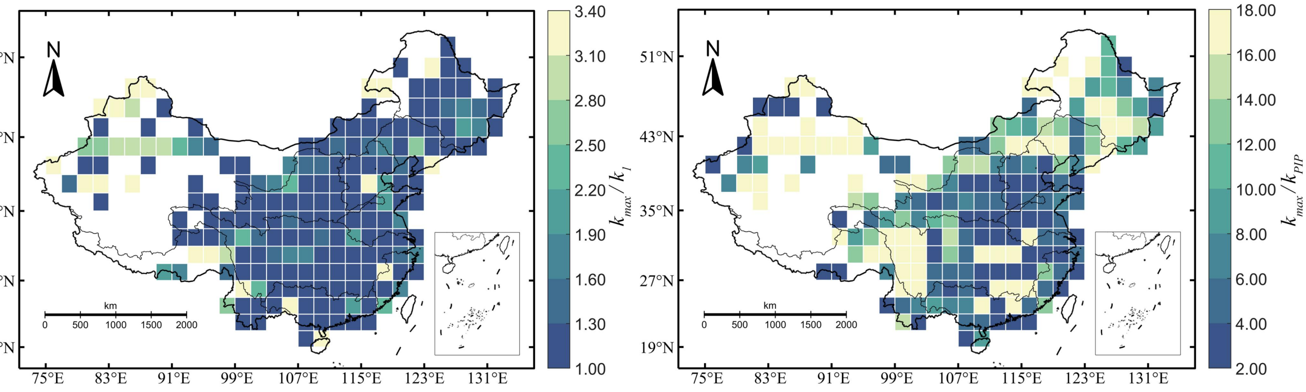

(a) (b)

Figure 10: Spatial distribution of the ratios in k from the perspective of Conceptual Model 1 ($t_{optimal} \rightarrow t_1$) and Conceptual Model 2 ($t_{optimal} \rightarrow t_{PIP}$). (a) The ratio of k between the t_c and t_1 (k_{max}/k_1), (b) the ratio of k between the t_c and t_{PIP} (k_{max}/k_{PIP}).

Table 2: Summary of the median values of k_{max}/k_1 and k_{max}/k_{PIP} across the ten river basins and all of China.

River basin	*P50* (k_{max}/k_1)	*P50* (k_{max}/k_{PIP})
Songhua River	1.000	12.555
Liao River	1.135	15.430
Northwestern Rivers	1.023	7.677
Hai River	1.000	2.413
Yellow River	1.001	4.932
Yangtze River	1.000	4.704
Huai River	1.000	3.707
Southeastern Rivers	1.000	3.428
Southwestern Rivers	1.069	6.539
Pearl River	1.000	3.429
All of China	1.000	6.979

Note: red and blue numbers indicate the maximum and minimum value of P_{50} for ten river basins in China, respectively.

https://doi.org/10.5194/egusphere-2025-4213
Preprint. Discussion started: 9 October 2025

5 Discussion

5.1 MYD mitigation response to increased precipitation

Current studies on precipitation-based drought mitigation have primarily focused on early intervention (DeChant and Moradkhani, 2015; Livneh and Hoerling, 2016; Wu et al., 2018). Yang et al. (2017) integrated early precipitation replenishment with drought-induced losses and concluded that earlier interventions are more effective in mitigating drought impacts. This is consistent with the discussion of Conceptual Model 1 in Section 3.4. However, due to the statistical properties of standardized drought indices, more severe drought conditions are often associated with higher mitigation efficiency under increased precipitation (Fig. 1). Zhang et al. (2024) highlighted that extremely dry conditions tend to exhibit a higher probability of drought recovery under the same level of increased precipitation. This finding can be explained by Conceptual Model 2 presented in Section 3.4. The nonlinear pattern in DS response to increased precipitation (Fig. 1 and Fig. 5) can be more comprehensively understood by jointly considering these two conceptual models. To further clarify this relationship, we derived response curves at different $t_{forcing}$ (Fig. 5) based on the DMQM developed in Section 3.4. Under the same precipitation forcing, a higher value of *k* at a given $t_{forcing}$ indicates greater mitigation efficiency. Our findings reveal that the $t_{optimal}$ of MYD ranges from t_1 to t_{PIP} (Fig. 10 and Table 2).

Consistent with several existing studies (Pan et al., 2013; Haile et al., 2020), t_1 remains the dominant $t_{optimal}$ across China. However, we noted that t_2 and t_3, while occurring later than t_1, are still non-negligible in the early stage of MYD. Spatially, the grids where t_2 and t_3 are dominant account for 22.11% and 11.06% of all grids, respectively (Fig. 6b). According to the classification of climate zones based on average annual precipitation (Yang et al., 2022), compared with the humid river basins in southern China, the arid and semi-arid northern regions exhibited a higher probability that mitigation efficiency in response to increased precipitation at t_2 and t_3 exceeds that at t_1 (Fig. 7 and Fig. 10a). We noticed that the Liao River basin (semi-arid basin) and Pearl River basin (humid basin) exhibited relatively high and low MYD mitigation efficiency, respectively. This may be attributed to the generally more severe drought conditions in the Liao River basin compared to those in the Pearl River basin (Huang et al., 2019; Lai et al., 2024; Zhang et al., 2025). Due to the characteristics of standardized drought indices (as discussed in Sections 1 and 3.4), increased precipitation tends to be more effective in mitigating drought impacts in the Liao River basin. This conclusion was consistent with previous findings (Zhang et al., 2024; Wang et al., 2025), showing the importance of earlier rainfall replenishment for mitigating MYD in the humid basins of China. In a word, understanding MYD mitigation responses to increased precipitation is essential for guiding more targeted and effective drought mitigation strategies, ensuring that interventions are both timely and regionally appropriate.

5.2 Factors influencing MYD mitigation efficiency

Recent studies have shown that droughts are increasing in both frequency and severity (Dai, et al., 2020; Fischer, et al., 2025; Gebrechorkos, et al., 2025). Similarly, Chen et al. (2025) highlighted that MYDs are also becoming more frequent and severe at global scales. To further characterize the dynamic evolution of MYD, three commonly used indices include DD,

https://doi.org/10.5194/egusphere-2025-4213
Preprint. Discussion started: 9 October 2025

DS, and DI. Among these, DD is a key factor for identifying MYDs, as MYDs are typically defined by a duration exceeding 12 months (Massari et al., 2022). DS represents the overall impact of MYD, while DI is related to the onset timing of the recovery stage. In current studies, standardized drought indices are commonly used to quantify drought severity (Mishra and Singh, 2010). According to the statistical characteristics of the normal distribution (Dai, 2011), drought indices responses to identical precipitation inputs can vary considerably depending on drought severity. This aligns with Conceptual Model 2 presented in Section 3.4, where small increases in precipitation have the potential to induce substantial shifts toward recovery when the index deviates far from zero. Our findings further indicate that t_1 and t_{PIP} of MYD do not coincide, especially in longer-duration MYD, where t_{PIP} tends to occur much later than t_1. With that in mind, we examined the relationship between DD and *k*. Our results demonstrate a positive correlation between DD and *k* in MYD (Fig. 8 and Fig. 9). Specifically, basins in northern China, characterized by longer DD, tend to have a higher probability of t_2 or t_3 being the $t_{optimal}$ in contrast to southern basins with shorter DD (Fig. 8 and Table 1).

5.3 Limitations and uncertainties

Droughts are not only influenced by *pr*, but also by other non-precipitation factors such as wind speed, air temperature, radiation, and relative humidity, among others. These non-precipitation factors are widely used to estimate potential evapotranspiration (Gebrechorkos et al., 2025). However, this study focuses solely on *pr*. This is primarily because drought mitigation mainly depends on the effective management and allocation of available water resources. In future studies, the performance of the framework could be further enhanced by considering these non-precipitation factors. It is essential to recognize that our study is a retrospective analysis based on historical MYDs. This study provides a framework for identifying $t_{optimal}$ at the early stage of MYD development in drought early warning systems. However, determining whether a drought event would develop into an MYD at an early stage remains a major challenge (Xu et al., 2021; Gumus, 2023). This challenge arises from the complexity of the factors influencing the development of droughts into MYDs. Furthermore, this study currently focuses solely on meteorological drought. Research on other types of drought, such as agricultural, hydrological, and socio-economic droughts, will also be a key focus in future studies. Future research should evaluate the applicability of our framework to other types of drought. To this end, it is also necessary to further optimize the framework by fully considering additional influencing factors (Tian et al., 2022; Wu et al., 2022; Meresa et al., 2023).

6 Conclusion

This study applied a series of numerical experiments involving *pr* gradient increases to investigate $t_{optimal}$ of drought mitigation for 351 historical MYDs across ten river basins in China, based on PDSI derived from daily meteorological data (1961-2020). Following these experiments, we developed the DMQM, a single-parameter model designed to quantify mitigation efficiency through the key coefficient, *k*, with $t_{optimal}$ identified as the timing corresponding to k_{max}. The main conclusions can be summarized as follows:

https://doi.org/10.5194/egusphere-2025-4213
Preprint. Discussion started: 9 October 2025

(1) We revealed a nonlinear response relationship between DS and precipitation forcing applied incrementally along a gradient. This nonlinear response is well characterized by the DMQM, as shown by close alignment between model estimates and actual values (slopes of 1.063, 1.060, and 1.037 for t_1, t_2, and t_3 along the 1:1 reference line), confirming its reliability in quantifying mitigation efficiency.

(2) While t_1 remains the dominant $t_{optimal}$ in most regions, accounting for 58.79% of all grids, t_2 and t_3 are also non-negligible, accounting for 22.11% and 11.06%, respectively. These findings indicate that although early-stage drought mitigation measures during t_1 is generally more effective in reducing drought risks, a non-negligible portion of grids suggest that t_1 is not always optimal, and delayed rainfall replenishment at t_2 or t_3 can yield better outcomes under certain conditions. Compared to the humid river basins in Southern China, the arid and semi-arid northern regions exhibited a higher probability that the k at t_2 or t_3 would exceed that at t_1.

(3) DD is a key factor for determining $t_{optimal}$ for drought mitigation, as MYDs are typically defined by a duration exceeding 12 months. Longer DD was associated with a greater likelihood of t_2 or t_3 being the $t_{optimal}$, evidenced by R^2 values of 0.526 and 0.578, respectively. When DD exceeds 29 months, the mitigation efficiencies of t_2 and t_3 become comparable to that of t_1. With the increasing frequency and severity of MYDs in the future, our findings can offer methodological guidance for designing more targeted and effective mitigation strategies, ensuring that rainfall replenishment measures are both timely and regionally appropriate.

Code availability

All MATLAB codes can be provided by the corresponding authors upon request.

Data availability

The daily meteorological dataset from 756 stations suitable for calculating PDSI during the period of 1961 to 2020 over China is available from the National Meteorological Information Center of the China Meteorological Administration via http://www.nmic.cn/.

Author contribution

Yichen Zhang: Conceptualization, Data curation, Formal analysis, Funding acquisition, Investigation, Methodology, Supervision, Validation, Visualization, Writing - original draft, Writing - review and editing. **Fubao Sun**: Conceptualization, Investigation, Methodology, Supervision, Writing - review and editing. **Wenbin Liu**: Conceptualization, Investigation, Formal analysis, Methodology, Validation, Writing - review and editing. **Jie Zhang**: Conceptualization, Formal analysis, Funding acquisition, Investigation, Methodology, Project administration, Resources, Supervision, Validation, Writing -

review and editing. **Wenli Lai**: Data curation, Investigation, Methodology, Project administration, Supervision. **Jiquan Lin**: Data curation, Investigation, Validation, Visualization. **Wenchao Sun**: Conceptualization, Formal analysis, Methodology. **Wenjie Liu**: Conceptualization, Methodology, Project administration. **Zhongyi Sun**: Data curation, Visualization. **Peng Wang**: Formal analysis, Validation.

Competing interests

The authors declare that they have no conflict of interest.

Acknowledgments

The authors express their gratitude to the National Natural Science Foundation of China, Hainan Province Science and Technology Special Fund, and the Innovative Research Projects for Postgraduates of Hainan Province for the financial support of this research project.

Financial support

This research has been supported by the National Natural Science Foundation of China (grant Nos. 41901043 and 42261005); Hainan Province Science and Technology Special Fund (grant No. ZDYF2023SHFZ092); and the Innovative Research Projects for Postgraduates of Hainan Province (grant No. Qhyb2024-100).

References

Ault, T.R.: On the essentials of drought in a changing climate, Science, 368, 256-260, doi: 10.1126/science.aaz5492, 2020.

Berdugo, M., Delgado-Baquerizo, M., Soliveres, S., Hernández-Clemente, R., Zhao, Y., Gaitán, J.J., Gross, N., Saiz, H., Maire, V., Lehmann, A., and Rillig, M.C.: Global ecosystem thresholds driven by aridity, Science, 367, 787-790, doi: 10.1126/science.aay5958, 2020.

Blauhut, V., Stahl, K., Stagge, J.H., Tallaksen, L.M., De Stefano, L., and Vogt, J.: Estimating drought risk across Europe from reported drought impacts, drought indices, and vulnerability factors, Hydrol. Earth Syst. Sci., 20 , 2779-2800, doi: https://doi.org/10.5194/hess-20-2779-2016, 2016.

Brunner, M.I. and Tallaksen, L.M.: Proneness of European catchments to multiyear streamflow droughts, Water Resour. Res., 55, 8881-8894, doi: https://doi.org/10.1029/2019WR025903, 2019.

Büntgen, U., Urban, O., Krusic, P.J., Rybníček, M., Kolář, T., Kyncl, T., Ač, A., Koňasová, E., Čáslavský, J., Esper, J., and Wagner, S.: Recent European drought extremes beyond Common Era background variability, Nat. Geosci., 14, 190-196, doi: https://doi.org/10.1038/s41561-021-00698-0, 2021.

Cavus, Y. and Aksoy, H.: Critical drought severity/intensity-duration-frequency curves based on precipitation deficit, J. Hydrol., 584, 124312, doi: https://doi.org/10.1016/j.jhydrol.2019.124312, 2020.

Chen, L., Brun, P., Buri, P., Fatichi, S., Gessler, A., McCarthy, M.J., Pellicciotti, F., Stocker, B. and Karger, D.N.: Global increase in the occurrence and impact of multiyear droughts, Science, 387, 278-284, doi: 10.1126/science.ado4245, 2025.

Dai, A.: Drought under global warming: a review, Wiley Interdiscip. Rev., 2, 45-65, doi: https://doi.org/10.1002/wcc.81, 2011.

Dai, A.: Increasing drought under global warming in observations and models, Nat. Clim. Change, 3, 52-58, doi: https://doi.org/10.1038/nclimate1633, 2013.

Dai, M., Huang, S., Huang, Q., Leng, G., Guo, Y., Wang, L., Fang, W., Li, P., and Zheng, X.: Assessing agricultural drought risk and its dynamic evolution characteristics, Agric. Water Manage., 231, 106003, doi: https://doi.org/10.1016/j.agwat.2020.106003, 2020.

DeChant, C.M. and Moradkhani, H.: Analyzing the sensitivity of drought recovery forecasts to land surface initial conditions, J. Hydrol., 526, 89-100, doi: https://doi.org/10.1016/j.jhydrol.2014.10.021, 2015.

Easterling, D.R., Wallis, T.W., Lawrimore, J.H., and Heim Jr, R.R.: Effects of temperature and precipitation trends on US drought, Geophys. Res. Lett., 34, L20709, doi: https://doi.org/10.1029/2007GL031541, 2007.

Feng, X., Wang, Z., Wu, X., Huang, S., Li, J., Lai, C., Zeng, Z., and Lin, G.: Tracking 3D drought events across global river basins: Climatology, spatial footprint, and temporal changes, Geophys. Res. Lett., 52, e2024GL111442, doi: https://doi.org/10.1029/2024GL111442, 2025.

Fischer, E.M., Bador, M., Huser, R., Kendon, E.J., Robinson, A., and Sippel, S.: Record-breaking extremes in a warming climate, Nat. Rev. Earth Environ., 6, 456-470, doi: https://doi.org/10.1038/s43017-025-00681-y, 2025.

Gebrechorkos, S.H., Sheffield, J., Vicente-Serrano, S.M., Funk, C., Miralles, D.G., Peng, J., Dyer, E., Talib, J., Beck, H.E., Singer, M.B., and Dadson, S.J.: Warming accelerates global drought severity, Nature, 642, 628-635, doi: https://doi.org/10.1038/s41586-025-09047-2, 2025.

Gu, L., Chen, J., Yin, J., Sullivan, S.C., Wang, H.M., Guo, S., Zhang, L., and Kim, J.S.: Projected increases in magnitude and socioeconomic exposure of global droughts in 1.5 and 2 °C warmer climates, Hydrol. Earth Syst. Sci., 24, 451-472, doi: https://doi.org/10.5194/hess-24-451-2020, 2020.

Gumus, V.: Evaluating the effect of the SPI and SPEI methods on drought monitoring over Turkey, J. Hydrol., 626, 130386, doi: https://doi.org/10.1016/j.jhydrol.2023.130386, 2023.

Gupta, A. and Karthikeyan, L.: Role of initial conditions and meteorological drought in soil moisture drought propagation: An event-based causal analysis over South Asia, Earth's Future, 12, e2024EF004674, doi: https://doi.org/10.1029/2024EF004674, 2024.

Haile, G.G., Tang, Q., Li, W., Liu, X., and Zhang, X.: Drought: Progress in broadening its understanding, Wiley Interdiscip. Rev.-Water, 7, e1407, doi: https://doi.org/10.1002/wat2.1407, 2020.

Hao, Z., Singh, V.P., and Xia, Y.: Seasonal drought prediction: Advances, challenges, and future prospects, Rev. Geophys., 56, 108-141, doi: https://doi.org/10.1002/2016RG000549, 2018.

Huang, S., Wang, L., Wang, H., Huang, Q., Leng, G., Fang, W., and Zhang, Y.: Spatio-temporal characteristics of drought structure across China using an integrated drought index, Agric. Water Manage., 218, 182-192, doi: https://doi.org/10.1016/j.agwat.2019.03.053, 2019.

Jacobi, J., Perrone, D., Duncan, L.L., and Hornberger, G.: A tool for calculating the Palmer drought indices, Water Resour. Res., 49, 6086-6089, doi: https://doi.org/10.1002/wrcr.20342, 2013.

Lai, C., Sun, H., Wu, X., Li, J., Wang, Z., Tong, H., and Feng, J.: Water availability may not constrain vegetation growth in Northern Hemisphere, Agric. Water Manage., 291, 108649, doi: https://doi.org/10.1016/j.agwat.2023.108649, 2024.

Lin, H., Yu, Z., Chen, X., Gu, H., Ju, Q., and Shen, T.: Spatial-temporal dynamics of meteorological and soil moisture drought on the Tibetan Plateau: Trend, response, and propagation process, J. Hydrol., 626, 130211, doi: https://doi.org/10.1016/j.jhydrol.2023.130211, 2023.

Liu, Y., Zhu, Y., Ren, L., Singh, V.P., Yang, X., and Yuan, F.: A multiscalar Palmer drought severity index, Geophys. Res. Lett., 44, 6850-6858, doi: https://doi.org/10.1002/2017GL073871, 2017.

Livneh, B. and Hoerling, M.P.: The physics of drought in the US central Great Plains, J. Clim., 29, 6783-6804, doi: https://doi.org/10.1175/JCLI-D-15-0697.1, 2016.

Luo, L., Apps, D., Arcand, S., Xu, H., Pan, M., and Hoerling, M.: Contribution of temperature and precipitation anomalies to the California drought during 2012–2015, Geophys. Res. Lett., 44, 3184-3192, doi: https://doi.org/10.1002/2016GL072027, 2017.

Ma, Q., Li, Y., Liu, F., Feng, H., Biswas, A., and Zhang, Q.: SPEI and multi-threshold run theory based drought analysis using multi-source products in China, J. Hydrol., 616, 128737, doi: https://doi.org/10.1016/j.jhydrol.2022.128737, 2023.

https://doi.org/10.5194/egusphere-2025-4213
Preprint. Discussion started: 9 October 2025

Mao, Y., Nijssen, B., and Lettenmaier, D.P.: Is climate change implicated in the 2013–2014 California drought? A hydrologic perspective, Geophys. Res. Lett., 42, 2805-2813, doi: https://doi.org/10.1002/2015GL063456, 2015.

Massari, C., Avanzi, F., Bruno, G., Gabellani, S., Penna, D., and Camici, S.: Evaporation enhancement drives the European water-budget deficit during multi-year droughts, Hydrol. Earth Syst. Sci., 26, 1527-1543, doi: https://doi.org/10.5194/hess-26-1527-2022, 2022.

McCabe, G.J. and Wolock, D.M.: Variability and trends in global drought, Earth Space Sci., 2, 223-228, doi: https://doi.org/10.1002/2015EA000100, 2015.

Meresa, H., Zhang, Y., Tian, J., and Faiz, M.A.: Understanding the role of catchment and climate characteristics in the propagation of meteorological to hydrological drought, J. Hydrol., 617, 128967, doi: https://doi.org/10.1016/j.jhydrol.2022.128967, 2023.

Mishra, A.K. and Singh, V.P.: A review of drought concepts, J. Hydrol., 391, 202-216, doi: https://doi.org/10.1016/j.jhydrol.2010.07.012, 2010.

Moravec, V., Markonis, Y., Rakovec, O., Svoboda, M., Trnka, M., Kumar, R., and Hanel, M.: Europe under multi-year droughts: how severe was the 2014–2018 drought period?, Environ. Res. Lett., 16, 034062, doi: 10.1088/1748-9326/abe828, 2021.

Mukherjee, S. and Mishra, A.K.: Increase in compound drought and heatwaves in a warming world, Geophys. Res. Lett., 48, e2020GL090617, doi: https://doi.org/10.1029/2020GL090617, 2021.

Palagi, E., Coronese, M., Lamperti, F., and Roventini, A.: Climate change and the nonlinear impact of precipitation anomalies on income inequality, Proc. Natl. Acad. Sci., 119, e2203595119, doi: https://doi.org/10.1073/pnas.2203595119, 2022.

Palmer, W.C.: Meteorological drought, Research paper no. 45, US Weather Bureau, Washington, DC, 58 pp., 1965.

Pan, M., Yuan, X., and Wood, E.F.: A probabilistic framework for assessing drought recovery, Geophys. Res. Lett., 40, 3637-3642, doi: https://doi.org/10.1002/grl.50728, 2013.

Shi, H., Tian, H., Lange, S., Yang, J., Pan, S., Fu, B., and Reyer, C.P.: Terrestrial biodiversity threatened by increasing global aridity velocity under high-level warming, Proc. Natl. Acad. Sci., 118, e2015552118, doi: https://doi.org/10.1073/pnas.2015552118, 2021.

Stevenson, S., Coats, S., Touma, D., Cole, J., Lehner, F., Fasullo, J., and Otto-Bliesner, B.: Twenty-first century hydroclimate: A continually changing baseline, with more frequent extremes, Proc. Natl. Acad. Sci., 119, e2108124119, doi: https://doi.org/10.1073/pnas.2108124119, 2022.

Tian, Q., Lu, J., and Chen, X.: A novel comprehensive agricultural drought index reflecting time lag of soil moisture to meteorology: A case study in the Yangtze River basin, China, Catena, 209, 105804, doi: https://doi.org/10.1016/j.catena.2021.105804, 2022.

Ullah, I., Ma, X., Asfaw, T.G., Yin, J., Iyakaremye, V., Saleem, F., Xing, Y., Azam, K., and Syed, S.: Projected changes in increased drought risks over South Asia under a warmer climate, Earth's Future, 10, e2022EF002830, doi: https://doi.org/10.1029/2022EF002830, 2022.

Van Dijk, A.I., Beck, H.E., Crosbie, R.S., De Jeu, R.A., Liu, Y.Y., Podger, G.M., Timbal, B., and Viney, N.R.: The Millennium Drought in southeast Australia (2001–2009): Natural and human causes and implications for water resources, ecosystems, economy, and society, Water Resour. Res., 49, 1040-1057, doi: https://doi.org/10.1002/wrcr.20123, 2013.

van Mourik, J., Ruijsch, D., van der Wiel, K., Hazeleger, W., and Wanders, N.: Regional drivers and characteristics of multi-year droughts, Weather Clim. Extremes, 48, 100748, doi: https://doi.org/10.1016/j.wace.2025.100748, 2025.

Vicente-Serrano, S.M., Domínguez-Castro, F., Beguería, S., El Kenawy, A., Gimeno-Sotelo, L., Franquesa, M., Azorin-Molina, C., Andres-Martin, M., and Halifa-Marín, A.: Atmospheric drought indices in future projections, Nat. Water., 3, 374-387, doi: https://doi.org/10.1038/s44221-025-00416-9, 2025.

Vicente-Serrano, S.M., Beguería, S., and López-Moreno, J.I.: A multiscalar drought index sensitive to global warming: the standardized precipitation evapotranspiration index, J. Clim., 23, 1696-1718, doi: https://doi.org/10.1175/2009JCLI2909.1, 2010.

Wang, C., Chen, J., Lee, S.C., Xiong, L., Su, T., Lin, Q., and Xu, C.Y.: Response and recovery times of vegetation productivity under drought stress: Dominant factors and relationships, J. Hydrol., 655, 132945, doi: https://doi.org/10.1016/j.jhydrol.2025.132945, 2025.

https://doi.org/10.5194/egusphere-2025-4213
Preprint. Discussion started: 9 October 2025

Wu, J., Chen, X., Yao, H., Liu, Z., and Zhang, D.: Hydrological drought instantaneous propagation speed based on the variable motion relationship of speed-time process, Water Resour. Res., 54, 9549-9565, doi: https://doi.org/10.1029/2018WR023120, 2018.

Wu, J., Yao, H., Chen, X., Wang, G., Bai, X., and Zhang, D.: A framework for assessing compound drought events from a drought propagation perspective, J. Hydrol., 604, 127228, doi: https://doi.org/10.1016/j.jhydrol.2021.127228, 2022.

Wu, W., Zhang, J., Sun, Z., Yu, J., Liu, W., Yu, R., and Wang, P.: Attribution analysis of land degradation in Hainan Island based on geographical detector, Ecol. Ind., 141, 109119, doi: https://doi.org/10.1016/j.ecolind.2022.109119, 2022.

Xu, L., Chen, N., Yang, C., Zhang, C., and Yu, H.: A parametric multivariate drought index for drought monitoring and assessment under climate change, Agric. For. Meteorol., 310, 108657, doi: https://doi.org/10.1016/j.agrformet.2021.108657, 2021.

Xu, Y., Zhu, X., Cheng, X., Gun, Z., Lin, J., Zhao, J., Yao, L., and Zhou, C.: Drought assessment of China in 2002–2017 based on a comprehensive drought index, Agric. For. Meteorol., 319, 108922, doi: https://doi.org/10.1016/j.agrformet.2022.108922, 2022.

Yang, L., Zhao, G., Tian, P., Mu, X., Tian, X., Feng, J., and Bai, Y.: Runoff changes in the major river basins of China and their responses to potential driving forces, J. Hydrol., 607, 127536, doi: https://doi.org/10.1016/j.jhydrol.2022.127536, 2022.

Yang, X., Wu, F., Yuan, S., Ren, L., Sheffield, J., Fang, X., Jiang, S., and Liu, Y.: Quantifying the impact of human activities on hydrological drought and drought propagation in China using the PCR-GLOBWB v2. 0 model, Water Resour. Res., 60, e2023WR035443, doi: https://doi.org/10.1029/2023WR035443, 2024.

Yang, Y., McVicar, T.R., Donohue, R.J., Zhang, Y., Roderick, M.L., Chiew, F.H., Zhang, L., and Zhang, J.: Lags in hydrologic recovery following an extreme drought: Assessing the roles of climate and catchment characteristics, Water Resour. Res., 53, 4821-4837, doi: https://doi.org/10.1002/2017WR020683, 2017.

Yevjevich, V.M.: An objective approach to definitions and investigations of continental hydrologic droughts. Hydro. Pap., Colorado State University, no. 23, 25 pp., 1967.

Zhang, J., Sun, F., Xu, J., Chen, Y., Sang, Y.F., and Liu, C.: Dependence of trends in and sensitivity of drought over China (1961–2013) on potential evaporation model, Geophys. Res. Lett., 43, 206-213, doi: https://doi.org/10.1002/2015GL067473, 2016.

Zhang, L., Yuan, F., and He, X.: Probabilistic assessment of global drought recovery and its response to precipitation changes, Geophys. Res. Lett., 51, e2023GL106067, doi: https://doi.org/10.1029/2023GL106067, 2024.

Zhang, Q., Miao, C., Su, J., Gou, J., Hu, J., Zhao, X., and Xu, Y.: A new high-resolution multi-drought-index dataset for mainland China, Earth Syst. Sci. Data, 17, 837-853, doi: https://doi.org/10.5194/essd-17-837-2025, 2025.

Zhang, W., Furtado, K., Wu, P., Zhou, T., Chadwick, R., Marzin, C., Rostron, J., and Sexton, D.: Increasing precipitation variability on daily-to-multiyear time scales in a warmer world, Sci. Adv., 7, eabf8021, doi: 10.1126/sciadv.abf8021, 2021.

Zhou, Z., Zhang, L., Chen, J., She, D., Wang, G., Zhang, Q., Xia, J., and Zhang, Y.: Projecting global drought risk under various SSP-RCP scenarios, Earth's Future, 11, e2022EF003420, doi: https://doi.org/10.1029/2022EF003420, 2023.